Structural basis of human kinesin-8 function and inhibition

Julia Locke[a,1], Agnel Praveen Joseph[a], Alejandro Peña[a], Martin M. Möckel[b,c,2], Thomas U. Mayer[b,c], Maya Topf[a], and Carolyn A. Moores[a,3]

[a]Institute of Structural and Molecular Biology, Department of Biological Sciences, Birkbeck College, London, WC1E 7HX, United Kingdom; [b]Department of Biology, University of Konstanz, D-78457 Konstanz, Germany; and [c]Konstanz Research School of Chemical Biology, University of Konstanz, D-78457 Konstanz, Germany

Edited by Yale E. Goldman, University of Pennsylvania/PMI, Philadelphia, PA, and approved September 29, 2017 (received for review July 7, 2017)

Kinesin motors play diverse roles in mitosis and are targets for antimitotic drugs. The clinical significance of these motors emphasizes the importance of understanding the molecular basis of their function. Equally important, investigations into the modes of inhibition of these motors provide crucial information about their molecular mechanisms. Kif18A regulates spindle microtubules through its dual functionality, with microtubule-based stepping and regulation of microtubule dynamics. We investigated the mechanism of Kif18A and its inhibition by the small molecule BTB-1. The Kif18A motor domain drives ATP-dependent plus-end microtubule gliding, and undergoes conformational changes consistent with canonical mechanisms of plus-end–directed motility. The Kif18A motor domain also depolymerizes microtubule plus and minus ends. BTB-1 inhibits both of these microtubule-based Kif18A activities. A reconstruction of BTB-1–bound, microtubule-bound Kif18A, in combination with computational modeling, identified an allosteric BTB-1–binding site near loop5, where it blocks the ATP-dependent conformational changes that we characterized. Strikingly, BTB-1 binding is close to that of well-characterized Kif11 inhibitors that block tight microtubule binding, whereas BTB-1 traps Kif18A on the microtubule. Our work highlights a general mechanism of kinesin inhibition in which small-molecule binding near loop5 prevents a range of conformational changes, blocking motor function.

kinesin | cryo-electron microscopy | inhibition | microtubule dynamics | mitosis

The mitotic spindle orchestrates chromosome segregation during cell division and thus safeguards chromosomal stability. The spindle is built from microtubules (MTs), polar polymers of αβ-tubulin heterodimers, and its organization and dynamics are driven by numerous molecular motors. Together with dyneins, members of the kinesin superfamily undertake diverse tasks during spindle assembly and through mitosis (1). Kinesins are ATP-dependent motors that can move along MTs, organize them, and modify their dynamics. Despite being defined by their conserved motor domains, sequence variations within individual kinesin superfamily members enable them to perform distinct, specialized functions within the mitotic machinery (2). Of the ∼40 kinesins encoded in the human genome, approximately one-half have roles in mitosis, emphasizing both the importance of these motors in cell division and the diversity of functions they perform (3).

Many mitotic kinesins organize MTs, or move cargo within the spindle, by directionally stepping as dimers along spindle MT tracks. However, a subset of kinesins are instead essential for regulating the length of spindle MTs and their dynamics. Kinesin-8 family members exhibit complex behaviors with respect to regulation of spindle MT dynamics, although their overall roles within the spindle appear to be relatively evolutionarily conserved. Kinesin-8s in most eukaryotes, including Kip3 [*Saccharomyces cerevisiae* (4–7)], Klp5/6 [*Schizosaccharomyces pombe* (8, 9)], and Klp67A [*Drosophila melanogaster* (10)), are involved in controlling spindle length and regulating chromosomal movements. Vertebrates express three kinesin-8 family members—Kif18A, Kif18B, and Kif19—each of which plays distinct regulatory roles. While Kif18A mainly functions during mitotic chromosome positioning by regulating kinetochore MT dynamics (11–13), Kif18B predominantly controls astral MTs (14, 15). Kif19A is a motile MT depolymerase involved in cilia length control (16). Several studies have shown that human Kif18A is associated with invasive breast cancer (17), and its overexpression is linked to an unfavorable prognosis in primary hepatocellular carcinoma (18) and colorectal cancer (19). Thus, Kif18A in particular is both a possible biomarker for cancer prognosis and a potential target for antimitotic therapies.

The extent to which similar kinesin-8 spindle functions reflect shared molecular properties is less clear. For example, budding yeast Kip3 displays highly processive plus-end–directed motility (5, 6, 20, 21), and fission yeast Klp5/6 can form heterodimers that walk processively to MT plus-ends (22). These yeast motors enrich at MT plus-ends and Kip3 disassembles MTs in a length dependent manner (6, 20). Klp5/6 can both couple cargo movement to MT depolymerization (22), and have also been shown to enhance MT

Significance

Kinesins are a superfamily of ATP-dependent motors important for many microtubule-based functions, including multiple roles in mitosis. Small-molecule inhibitors of mitotic kinesins disrupt cell division and are being developed as antimitotic therapies. We investigated the molecular mechanism of the multitasking human mitotic kinesin Kif18A and its inhibition by the small molecule BTB-1. We used cryo-electron microscopy to visualize nucleotide-dependent conformational changes in microtubule-bound Kif18A, and the conformation of microtubule-bound, BTB-1-bound Kif18A. We calculated a putative BTB-1–binding site and validated this site experimentally to reveal the BTB-1 inhibition mechanism. Our work points to a general mechanism of kinesin inhibition, with wide implications for a targeted blockade of these motors in both dividing and interphase cells.

Author contributions: J.L., M.M.M., T.U.M., M.T., and C.A.M. designed research; J.L., A.P.J., A.P., and M.M.M. performed research; A.P.J., A.P., and M.T. contributed new reagents/analytic tools; J.L., A.P.J., A.P., M.M.M., and M.T. analyzed data; and J.L., A.P.J., T.U.M., M.T., and C.A.M. wrote the paper.

The authors declare no conflict of interest.

This article is a PNAS Direct Submission.

Data deposition: The cryo-EM reconstructions reported in this paper have been deposited in the Electron Microscopy Data Bank [accession nos. 3778 (NN), 3780 (AMPPNP), and 3803 (BTB-1)]. The docked coordinates reported in this paper have been deposited in the Protein Data Bank [accession nos. 5OAM (NN), 5OCU (AMPPNP), and 5OGC (BTB-1)].

[1]Present address: The Francis Crick Institute, Macromolecular Machines Laboratory, London NW1 1AT, United Kingdom.

[2]Present address: Institute of Molecular Biology (gGmbH) (IMB), Mainz 55128, Germany.

[3]To whom correspondence should be addressed. Email: c.moores@mail.cryst.bbk.ac.uk.

This article contains supporting information online at www.pnas.org/lookup/suppl/doi:10.1073/pnas.1712169114/-/DCSupplemental.

nucleation and induce catastrophe at MT ends (23). Although vertebrate kinesin-8s all display plus-end directed motility with robust processivity (16, 24–26), reports concerning their ability to modulate MT dynamics vary. For dimeric Kif18A, both active depolymerization (11) and antagonism of MT assembly have been reported (25, 27, 28). We previously showed that a monomeric human Kif18A construct is able to depolymerize MTs in vitro, albeit to a limited extent, as evidenced by tubulin ring formation in the presence of the nonhydrolyzable ATP analog AMPPNP (29). A more recent study of a mouse Kif19A monomeric construct described MT depolymerization activity and the capacity to generate ATP-dependent motility for this protein (30). Overall, it remains challenging to rationalize these disparate findings concerning the molecular properties and mechanisms of kinesin-8s. It also is not known whether recent descriptions of subdomain rearrangements in the motor domain of kinesin-1 on MT and nucleotide binding apply to the putatively multitasking motor domains of kinesin-8s (31, 32). Therefore, further dissection of the molecular mechanism of human kinesin-8s is crucial to understand their activities in the context of their mitotic roles in regulating MT dynamics. Small-molecule inhibitors can provide valuable insight into such mechanistic dissection.

While many current anticancer therapeutics are MT-binding agents—for example, the blockbuster drug Taxol (33)—mitotic kinesins have also been considered important chemotherapeutic targets for some time (34). Human kinesin-5, Kif11 [HsKif11, Kinesin Spindle Protein (KSP), Eg5], which contributes to formation and maintenance of spindle bipolarity, was the first mitotic kinesin for which specific small-molecule inhibitors were identified (35). Multiple HsKif11-specific inhibitors that cause collapse of the bipolar spindle, mitotic arrest, and cell death have since been identified (36). The best-studied HsKif11 inhibitors are allosteric inhibitors, which target an HsKif11-specific insert in loop5 (L5) within its motor domain. Binding of these compounds stabilizes a conformation that prevents tight binding of the motor to MTs and blocks its ability to generate force within the spindle. The study of such inhibitors also provides vital information about the molecular mechanism of Kif11 (34, 37).

Recently, the small molecule BTB-1 has been identified as an inhibitor that specifically inhibits Kif18A (38). Interestingly, and in contrast to many HsKif11 inhibitors, it acts on MT-bound Kif18A. Inhibitors that are specific for kinesin-MT complexes may be particularly advantageous as antimitotics, because the trapped MT-motor complexes may also sterically or mechanically block the activities of other motors in the spindle, amplifying the antimitotic effect. However, the precise mechanism of Kif18A inhibition by BTB-1 is not well understood. Elucidation of the inhibitory mechanism of BTB-1 is crucial to allow rational development of Kif18A-specific inhibitors, will shed light on the function of Kif18A in mitosis, and will provide further insight into mechanisms of kinesin motor function.

In this study, we therefore investigated the molecular mechanism of human Kif18A and its mode of inhibition by BTB-1. Using monomeric Kif18A motor domain constructs (Fig. 1*A*), we measured steady-state ATPase rates and multimotor gliding activities, where plus-end–directed motility was observed. Subnanometer-resolution cryo-EM reconstructions of the MT-bound Kif18A motor domain in the presence and absence of the nonhydrolyzable ATP analog AMPPNP showed nucleotide-dependent conformational changes that are consistent with subdomain rearrangements seen in other plus-end–directed kinesins (31, 32, 39). In addition, using total internal reflection fluorescence (TIRF) microscopy, we observed depolymerization of Taxol-stabilized MTs from both ends. We also captured tubulin ring/Kif18A complexes in 2D at subnanometer resolution, shedding light on its depolymerization mechanism. BTB-1 inhibited Kif18A ATPase, gliding, and depolymerization activities (38). Finally, the BTB-1 inhibition mechanism allowed us to determine the structure of the MT-bound

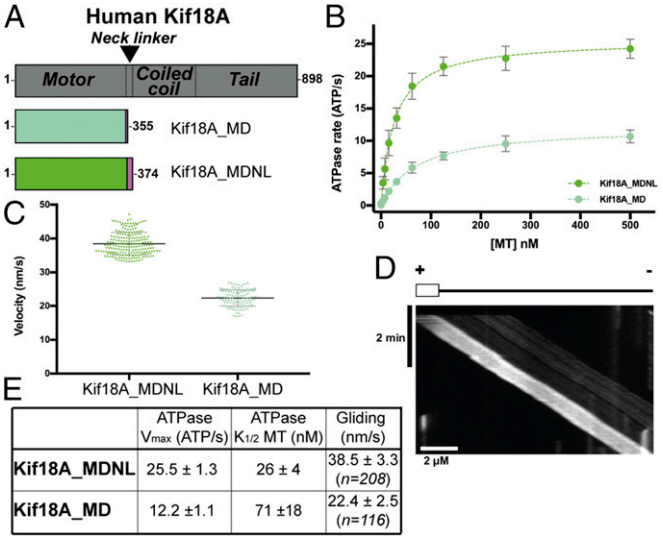

	ATPase V_{max} (ATP/s)	ATPase $K_{1/2}$ MT (nM)	Gliding (nm/s)
Kif18A_MDNL	25.5 ± 1.3	26 ± 4	38.5 ± 3.3 (*n=208*)
Kif18A_MD	12.2 ±1.1	71 ±18	22.4 ± 2.5 (*n=116*)

Fig. 1. ATPase and motile activities of Kif18A motor domain constructs. (*A*) Schematic of human Kif18A and the constructs, Kif18A_MD (light green) and Kif18A_MDNL (green), used in this study, with the neck linker indicated in pink. (*B*) MT-stimulated ATPase activity of Kif18A_MD and Kif18A_MDNL. Values are mean ± SD. (*C*) MT gliding velocity of Kif18A_MD and Kif18A_MDNL. The scatterplot shows all data, with mathematical mean ± SD indicated by horizontal bars. (*D*) Exemplar kymograph demonstrating plus-end–directed MT gliding driven by Kif18A_MDNL using polarity-marked MTs. (*E*) Summary table of ATPase and gliding assay parameters for each construct.

motor domain in complex with BTB-1. By combining 3D image processing and computational modeling approaches including small-molecule docking, we identified a putative binding site for BTB-1 and validated it experimentally.

The BTB-1–binding pocket lies at the junction of two subdomains within the Kif18A motor domain. BTB-1 thereby inhibits nucleotide-dependent subdomain rearrangements within Kif18A that block both motility and MT depolymerization. Although this binding site is in close proximity to where the allosteric inhibitors bind in HsKif11, BTB-1 selectively binds the MT-bound conformation of Kif18A close to Kif18A-specific residues. This work points to a general mode of kinesin inhibition, in which small molecules prevent subdomain rearrangements by binding at the subdomain interface of the kinesin motor domain, either trapping the motor on MTs or preventing MT binding.

Results

Enzyme and Motile Activities of Monomeric Kif18A. To understand the mechanism of Kif18A and its inhibition, we first measured the MT-stimulated ATPase activities of a monomeric Kif18A motor-neck linker construct, Kif18A_MDNL, and compared its activity with that of a previously studied truncated construct, Kif18A_MD. Fits of the data to a Michaelis–Menten function showed that the v_{max} of Kif18A_MDNL (25.5 ATP/s) was twice that of Kif18A_MD (12.2 ATP/s) while its affinity for MTs was approximately threefold tighter ($K_{1/2}$ = 26 nM for Kif18A_MDNL, vs. 71 nM for Kif18A_MD) (Fig. 1*B*). These data are in line with our previous analysis of a construct similar to Kif18A_MD (v_{max} = 17 ATP/s; $K_{1/2}$ = 110 nM; ref. 29). Our current data show that the presence of the complete Kif18A neck linker sequence in Kif18A_MDNL enhances the ATPase activity and MT affinity of the Kif18A monomer.

We also compared the activities of these two constructs in in vitro MT gliding assays. Intriguingly, both constructs supported ATP-dependent plus-end–directed motility (Fig. 1 *C* and *D*), but mean MT gliding velocity by Kif18A_MDNL (38.5 ± 3.3 nm/s; n = 208)

was faster than that by Kif18A_MD (22.4 ± 2.5 nm/s; n = 116) (t test, $P < 0.0001$). As expected (40), both monomer constructs drove slower gliding motility than are typically seen for Kif18A dimers (~100–200 nm/s; refs. 24, 25, 27); however, a complete neck linker sequence supported more robust motility (Fig. 1*C*), consistent with the central role of the neck linker in coupling motor ATPase activity to functional output in plus-end kinesins (40, 41) (Fig. 1*E*).

MT-Bound Kif18A_MDNL Undergoes Conformational Changes on ATP Binding. Using the more active Kif18A_MDNL construct, we used cryo-EM and image reconstruction to visualize the MT-bound Kif18A_MDNL in the absence of nucleotide [no nucleotide (NN) using apyrase treatment] and in an ATP-like conformation (using the nonhydrolyzable ATP analog AMPPNP) at ~6-Å resolution (Fig. 2 and *SI Appendix*, Fig. S1 *A* and *B*). The asymmetric unit of these reconstructions is Kif18A_MDNL bound to an αβ-tubulin dimer within the MT (Fig. 2*A*). To facilitate interpretation of our reconstructions, we calculated comparative models for each nucleotide state and refined them in the cryo-EM density using flexible fitting with Flex-EM (42) (Fig. 2 and *SI Appendix*, Fig. S1*C*).

In both structures, the contact between motor and MT is centered over the intradimer interface of the αβ-tubulin heterodimer, as seen previously for Kif18A_MD, Kif19A, as well as other kinesin-MT reconstructions (29–32, 39) (Fig. 2*A*). Helix-α4 extends continuously across the motor at the tubulin intradimer interface, and its N terminus forms part of the nucleotide-binding pocket. Three conserved structural elements around the nucleotide-binding pocket—the P-loop, switch I (loop9), and switch II (loop11) regions—respond to the nucleotide state of the motor (Fig. 2*B*).

In the NN reconstruction, the nucleotide-binding pocket is empty (Fig. 2*B*, *Left*, dotted blue circle). Density corresponding to loop11 (red) is visible and extends from the body of the motor, where it forms a single helical turn contacting the MT surface, before leading into helix-α4. Density corresponding to loop9 (yellow) is only partially visualized in this structure, which is consistent with the partial flexibility observed in other nucleotide-free MT/tubulin-bound kinesin structures (31, 32, 39). As was shown previously, many of these elements are not visible in the Kif18A_MD crystal structure (Protein Data Bank ID code 3LRE) (29), and become ordered on binding of the MT. As was also shown for Kif18A_MD and the motor domain of Kif19 (30), binding of MTs by Kif18A_MDNL also promotes a shift of helix-α3. This moves helix-α3 away from helix-α2 relative to its position in the ADP-bound crystal structure (*SI Appendix*, Fig. S2).

In addition to the C terminus of loop11 and helix-α4 at the intradimer tubulin interface, contacts are formed between Kif18A and the MT surface via β-sheet5/loop8, loop12, and helix-α5. Kinesin-8 sequences have a characteristic highly extended loop2 sequence. In this ~6-Å structure at higher thresholds, no distinct density corresponding to loop2 is observed forming an additional connection to the MT surface. This suggests flexibility in this region of the motor (Fig. 2*D*). However, when the current reconstruction is visualized using a more inclusive threshold, density forming a connection between the Kif18A_MDNL via its loop2 and MT surface can be seen (*SI Appendix*, Fig. S3). This is consistent with the previously calculated structure of Kif18A_MD at lower resolution (29), and with functional data concerning the importance of loop2 residues in Kif18A-MT interaction and function (43). The β-sheet1 subdomain, which contains loop2, lies above helix-α6, from which the motor's neck linker extends (Fig. 2*D*). In the NN reconstruction, the position of helix-α6 with respect to helix-α4 prevents neck linker docking, and no density corresponding to the neck linker is visible in this nucleotide state (Fig. 2 *C* and *D*, magenta arrow).

In the presence of AMPPNP, the nucleotide-binding site is clearly occupied by the bound nucleotide, and the closure of the

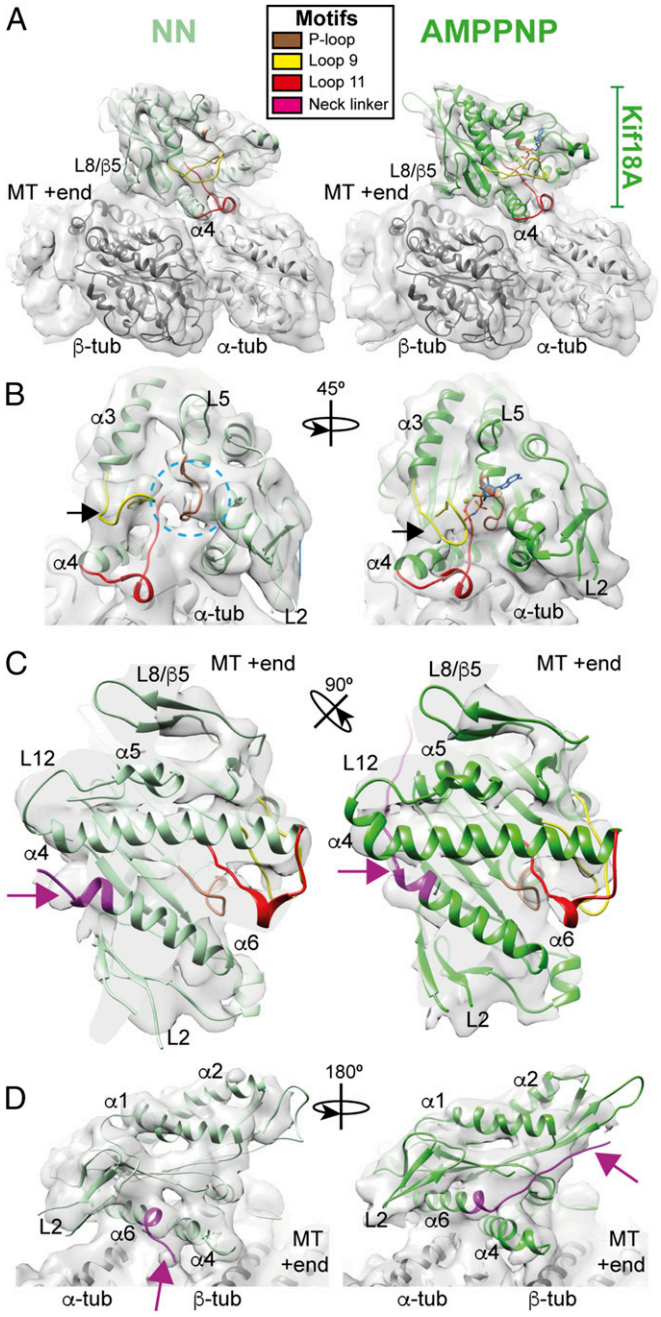

Fig. 2. Conformational changes in the Kif18A motor domain in response to ATP binding by cryo-EM. (*A*) Asymmetric unit from the Kif18_MDNL NN reconstruction (*Left*) and AMPPNP reconstruction (*Right*) contoured to show secondary structure elements. The cryo-EM densities are shown as a gray surface, the NN model is shown in light-green ribbons, the AMPPNP model in medium-green ribbons, and α- and β-tubulin are shown in light- and dark-gray ribbons, respectively. (*B*) The nucleotide-binding pocket of Kif18A_MDNL of the NN reconstruction (*Left*, dotted blue circle) and AMPPNP reconstruction (*Right*, AMPPNP shown in ball-and-stick depiction). The black arrow indicates loop9 (yellow) and its movement in response to AMPPNP; the indicated rotation relates views in *A* and *B*. (*C*) The MT-binding interface viewed from the MT toward Kif18A_MDNL of the NN reconstruction (*Left*) and AMPPNP reconstruction (*Right*), showing relatively few changes in response to AMPPNP binding. The arrow indicates the C terminus of helix-α6 and its transition to the neck linker (magenta); the indicated rotation relates views *A* and *C*. (*D*) Conformational changes of helix-α6 in the NN reconstruction (*Left*) and AMPPNP reconstruction (*Right*) alter MT connectivity and neck linker docking in response to AMPPNP binding (magenta arrow); the indicated rotation relates views in *A* and *D*.

conserved structural elements can be observed in response to the ATP analog (Fig. 2*B*, *Right*). While much of the MT-binding interface of Kif18A_MDNL remains stable in the transition between NN and AMPPNP (Fig. 2*C*, *Right*), the local conformational changes at the nucleotide-binding site coincide with larger structural rearrangements within the motor. In particular, on AMPPNP binding, helix-α6 extends and inserts between helix-α4 and the central beta sheet of the motor domain, resulting in redirection of the neck linker along the body of the Kif18A motor domain toward the MT plus-end (Fig. 2*D*, *Right*, magenta arrow). This is consistent with our observation that Kif18A_MDNL drives plus-end–directed motility in a gliding assay (Fig. 1*D*).

Overall, the structural comparison between the Kif18A_MDNL in the NN and AMPPNP reconstructions shows that the motor domain undergoes conformational changes on ATP binding, which are essential for plus-end–directed motility along MTs. Such conformational changes likely arise from rearrangements in three subdomains within the Kif18A motor domain, as described for kinesin-1 (31, 32) (*SI Appendix*, Fig. S4). The models calculated for the NN and AMPPNP states of Kif18_MDNL incorporate these subdomain rearrangements, such that (*i*) the so-called tubulin-binding subdomain corresponds to the relatively static regions of contact between motor and MT (Fig. 2*C*); (*ii*) the so-called SwitchI/II subdomain contains the Switch I/II sequences and surrounding secondary structural elements, including loop9, loop11, and helix-α3; and (*iii*) the so-called P-loop contains the rest of the motor, including helix-α6 and the neck linker. Thus, the Switch I/II and P-loop subdomains move with respect to each other and to the tubulin-binding subdomain once Kif18A_MDNL binds MTs (*SI Appendix*, Fig. S4) and AMPPNP, allowing neck linker docking.

MT Depolymerization by Kif18A_MDNL. The conformational changes described above are in line with the plus-end–directed MT motility driven by Kif18A monomers and similar to those exhibited by other plus-end kinesins. Nevertheless, we were intrigued to also compare the MT depolymerization activity of both our monomeric constructs. Although it is unclear whether the cellular roles of Kif18A depend on MT depolymerization activity or on the motor's ability to simply dampen dynamics at MT ends, we previously showed that Kif18A_MD could release tubulin from paclitaxel-stabilized MTs. This observation is consistent with the ability of the Kif18A motor domain to depolymerize MTs (29). To investigate this further, we used TIRF microscopy to directly visualize depolymerization of fluorescently labeled MTs by Kif18A_MDNL and Kif18A_MD (Fig. 3 *A* and *B*). In all cases, the observed depolymerization occurs from both plus-ends and minus-ends of the stabilized MTs. This can be explained by the monomeric nature of the construct, as it can diffuse in solution to either end of the MT in the TIRF assay and stimulate MT destabilization at both ends. The rates at which different MTs depolymerize in these assays are not uniform, and investigations of the origin of this variability are ongoing. Nevertheless, confirming and extending our previous study, we observed that both Kif18A_MD and Kif18A_MDNL shorten paclitaxel-stabilized MTs in the presence of AMPPNP. However, Kif18A_MDNL depolymerizes MT approximately threefold faster than Kif18A_MD, with mean depolymerization rates of 1.30 ± 0.70 nm/s (n = 119) and 0.37 ± 0.28 nm/s (n = 208) respectively (*t* test, $P < 0.0001$). In the presence of ATP, no MT depolymerization by Kif18_MD was observed, but Kif18A_MDNL did support ATP-dependent MT depolymerization, albeit more slowly than in the presence of AMPPNP [mean rate, 0.87 ± 0.43 nm/s (n = 99) (*t* test, $P < 0.0001$)]. Thus, the presence of the full neck linker sequence in Kif18A_MDNL enhances the depolymerization capacity of the Kif18A monomer.

Consistent with its higher depolymerization activity, we also observed formation of a larger number of curved Kif18A_MDNL-tubulin oligomers from paclitaxel-stabilized MTs compared with Kif18A_MD in the presence of AMPPNP (*SI Appendix*, Fig. S5 *A* and *B*). These oligomers include tubulin rings, which are built from a single curved protofilament. Both constructs showed a similar extent of binding to the MT lattice at the saturating motor concentrations used for these experiments. Thus, Kif18A_MDNL is substantially more active than Kif18A_MD in terms of MT depolymerization and tubulin ring formation.

To further investigate the structure of Kif18A_MDNL in the context of these curved tubulin structures, we imaged Kif18A_MDNL-tubulin rings using cryo-EM (Fig. 3*C*). Due to a preferred en face orientation of the rings in vitreous ice, we were not able to determine their 3D structure. Nevertheless, the 2D

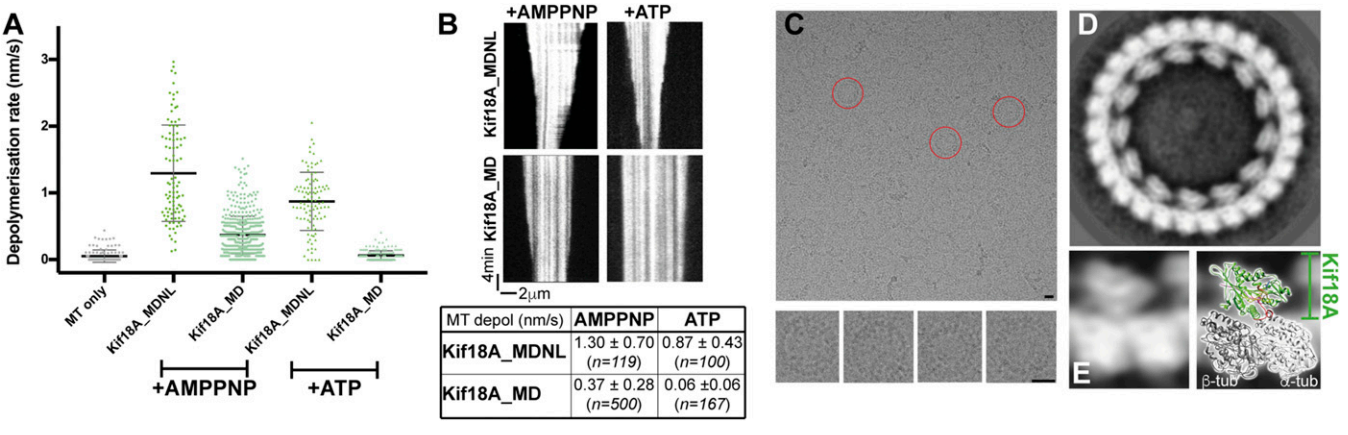

MT depol (nm/s)	AMPPNP	ATP
Kif18A_MDNL	1.30 ± 0.70 (*n=119*)	0.87 ± 0.43 (*n=100*)
Kif18A_MD	0.37 ± 0.28 (*n=500*)	0.06 ±0.06 (*n=167*)

Fig. 3. MT depolymerization by Kif18A monomers. (*A*) Scatterplot of the rate of depolymerization of paclitaxel-stabilized MTs by Kif18A constructs in the presence of AMPPNP or ATP measured using TIRF microscopy, with mean ±SD indicated by horizontal bars. (*B*) Representative kymographs showing depolymerization of paclitaxel-stabilized MTs by Kif18A monomeric constructs as indicated. (*C*, *Top*) Raw cryo-EM image showing tubulin rings formed by Kif18A_MDNL in the presence of AMPPNP. Individual rings, equivalent to the curvature of single protofilaments, are indicated by dotted red circles. (Scale bar: 10 nm.) (*C*, *Bottom*) Cryo-EM images of individual Kif18_MDNL-tubulin rings formed in the presence of AMPPNP. (Scale bar: 10 nm.) (*D*) 2D class average of Kif18A_MDNL-tubulin rings composed of 13 copies of the Kif18A_MDNL (inner ring of discrete densities) in complex with curved αβ-tubulin heterodimers (outer ring of continuous density). (*E*) 2D projection of an individual Kif18A_MDNL-tubulin dimer complex extracted from the ring class average (*Left*), and superposition of Kif18A_MDNL-MT atomic model on this density (*Right*), with Kif18A_MDNL in green, α-tubulin in light gray, and β-tubulin in dark gray, viewed toward the nucleotide-binding pocket. This highlights the good correspondence in these complexes apart from the curvature of the tubulin.

analysis of these rings yields a detailed view of these motor-tubulin complexes (Fig. 3*D*). They show that Kif18A_MDNL binds to curved αβ-tubulin dimers with a 1:1 stoichiometry, as was previously observed at low resolution for Kif18_MD (29). Most of the rings were composed of 13 or 14 Kif18A-tubulin dimers, but 12 copies of the motor-tubulin complex were also seen in the ring population (*SI Appendix*, Fig. S5*C*). This suggests that there may be some variation in the tubulin curvature induced by Kif18_MDNL, and thus in how many copies of the motor-tubulin complex can be accommodated in the closed rings that we used for the image analysis. However, the detailed view of the complex shows that the Kif18A_MDNL retains a compact conformation when bound to curved tubulin, similar to its configuration when bound to the straight MT lattice (Fig. 3*E*, *Left*).

To understand this in more detail, we matched a projection of tubulin-bound Kif18A_MDNL atomic model with the density of our 2D classes (Fig. 3*E*, *Right*). The excellent match of these two projection views suggests that the same structural elements within Kif18A_MDNL are responsible for binding to the curved tubulin conformation as bind to the straight MT lattice, centered around helix-α4 within the tubulin-binding subdomain. This also supports the conclusion that Kif18A_MDNL undergoes a relatively limited global rearrangement to adopt its depolymerizing conformation. These analyses imply that, due to the relative freedom of tubulin at MT ends, Kif18A_MDNL is able to induce or stabilize tubulin dimer curvature. In the presence of the nonhydrolyzable ATP analog AMPPNP, motor-tubulin complexes can be trapped and visualized.

Inhibition of Kif18A Activities by BTB-1. The small molecule BTB-1 (38) specifically inhibits Kif18A when bound to MTs and kinetically shows an ATP-competitive mode of inhibition. To further probe the effects of BTB-1 inhibition on our Kif18A constructs, we tested its effect on their ATPase, depolymerase, and gliding activities. Titration of increasing concentrations of BTB-1 inhibited the steady-state ATPase activities of both Kif18A_MD and Kif18A_MDNL. Thus, despite the different activities of these two constructs (Fig. 1*A*), both were inhibited by BTB-1 to the same extent (IC_{50} = 0.59 μM in MD and 0.61 μM in MDNL) (Fig. 4*A*), very close to the previously published value (38). Similarly, addition of BTB-1 to the depolymerization assay resulted in complete inhibition of Kif18A_MDNL activity (Fig. 4*B*). Furthermore, BTB-1 also showed an inhibitory effect on the ATP-dependent gliding activities of Kif18A_MDNL and Kif18A_MD (Fig. 4*C*). Titration of increasing concentrations of BTB-1 inhibited the gliding activity of Kif18A_MDNL (IC_{50} = 1.31 μM) (Fig. 4*D*), paralleling the inhibition observed in the ATPase assay (Fig. 4*A*). Importantly, MT gliding activity driven by Kif18A_MDNL could be fully restored by washing out the drug in the presence of ATP (*SI Appendix*, Fig. S6). This confirms the previous finding (38) that inhibition of Kif18A by BTB-1 is reversible. Taken together, these results suggest that all of the measured activities are linked by a common step that is blocked in the presence of BTB-1.

Structure of MT-Bound Kif18A_MDNL in Complex with BTB-1. Since BTB-1 is specific for Kif18A in the presence of MTs, we were able to determine the structure of MT-bound Kif18A_MDNL in the presence of BTB-1 by cryo-EM. This structure, with an overall resolution 4.8 Å (Fig. 5 and *SI Appendix*, Fig. S7*A*), allowed us to shed light on the inhibition mechanism of BTB-1. Although the resolution of the Kif18A_MDNL density is slightly worse than the overall resolution (*SI Appendix*, Fig. S7*A*), the resolution gradient between MT and motor is less prominent than in the NN and AMPPNP reconstructions, possibly due to stabilization of the motor on drug binding. Using this density, we calculated a model of the drug-bound conformation of Kif18A_MDNL (*SI Appendix*, Fig. S7*B*). Overall, the conformation of Kif18A_MDNL in the presence of BTB-1 is very similar to the conformation of Kif18A_MDNL NN (Fig. 5 *A* and *B*), including a very similar conformation of helix-α6 and a lack of density corresponding to the neck linker, indicating that the neck linker is not docked in this structure (Fig. 5*C*, magenta arrow). The nucleotide-binding pocket contains no density, indicative of the absence of bound nucleotide or BTB-1 itself (Fig. 5*B*, blue dotted circle).

When comparing BTB-1 and NN conformations of Kif18A_MDNL, only small conformational differences are seen around the nucleotide-binding pocket, with conformational shifts in the P-loop, helix-α2a, loop9, loop11, and the N terminus of helix-α4 (Fig. 5*B*). Thus, BTB-1 appears to trap Kif18A_MDNL in an NN-like conformation. While the nucleotide-binding site is open and in principle available to receive incoming ATP in the

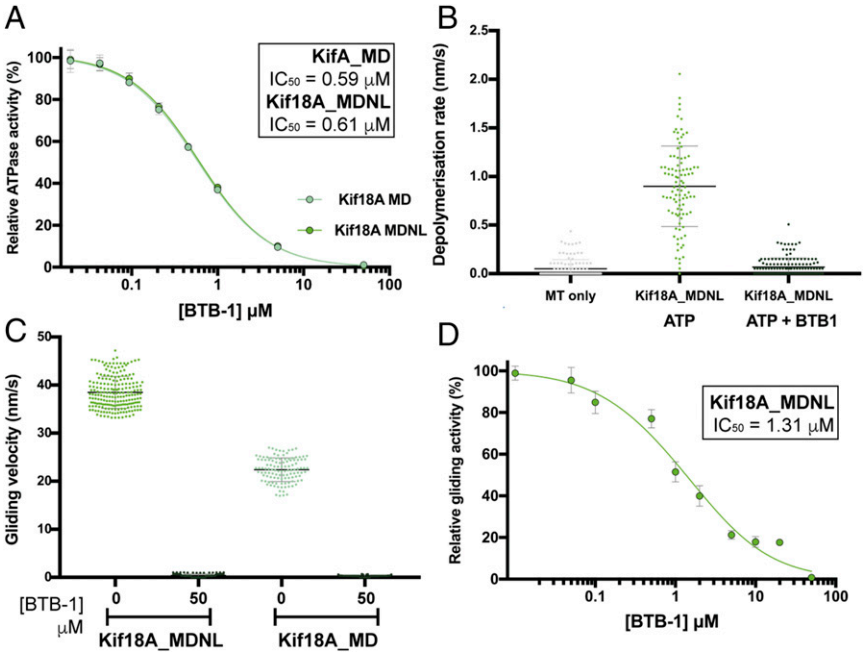

Fig. 4. Inhibition of Kif18A activities by BTB-1. (*A*) Equivalent inhibition of Kif18A_MD (at 30 nM) and Kif18A_MDNL (at 15 nM) ATPase activity by BTB-1 titration. The mathematical mean and SD are plotted for each condition with the curve fit (*SI Appendix, Materials and Methods*). In each case, R^2 = 0.999. (*B*) BTB-1 inhibits ATP-dependent MT depolymerization by Kif18A_MDNL (at 500 nM). Shown is a scatterplot of all the data, with mean ± SD indicated by horizontal bars. Data in the absence of BTB-1 are the same as in Fig. 3*A*. (*C*) Equivalent inhibition of Kif18A_MD and Kif18A_MDNL gliding activity by BTB-1. Shown is a scatterplot of all data, with mathematical mean ± SD indicated by horizontal bars. Data in the absence of BTB-1 are the same as in Fig. 1*C*. (*D*) Inhibition of Kif18A_MDNL gliding activity by BTB-1 titration. The mathematical mean ± SD are plotted for each condition with the curve fit; R^2 = 0.985. Data in the absence of BTB-1 are the same as in Fig. 1*C*.

presence of BTB-1, the conformational changes observed in the NN-AMPPNP transition that support MT gliding and formation of curved tubulin complexes seem to be blocked. Thus, our structure suggests that the kinetically ATP-competitive inhibition of Kif18A by BTB-1 occurs through an allosteric structural mechanism.

Molecular Mechanism of BTB-1 Inhibition of Kif18A. To further understand the mechanism of Kif18A inhibition by BTB-1 (Fig. 6*A*), we used TEMPy (44) to calculate the difference map between the BTB-1–bound and the NN Kif18A_MDNL cryo-EM reconstructions (Fig. 6*B*, orange density). As expected, some regions of difference density corresponded to areas of conformational change between the two conformations of Kif18A_MDNL in the vicinity of the nucleotide-binding pocket (Fig. 5*B*). In addition, however, the difference density also included a prominent and discrete peak between helix-α2 and helix-α3 (Fig. 6*B*, arrow), which was unoccupied by the fitted atomic model. Remarkably, this region corresponds to one of the well-described binding sites of Kif11 inhibitors (34), and lies at the junction of the Switch I/II and P-loop subdomains.

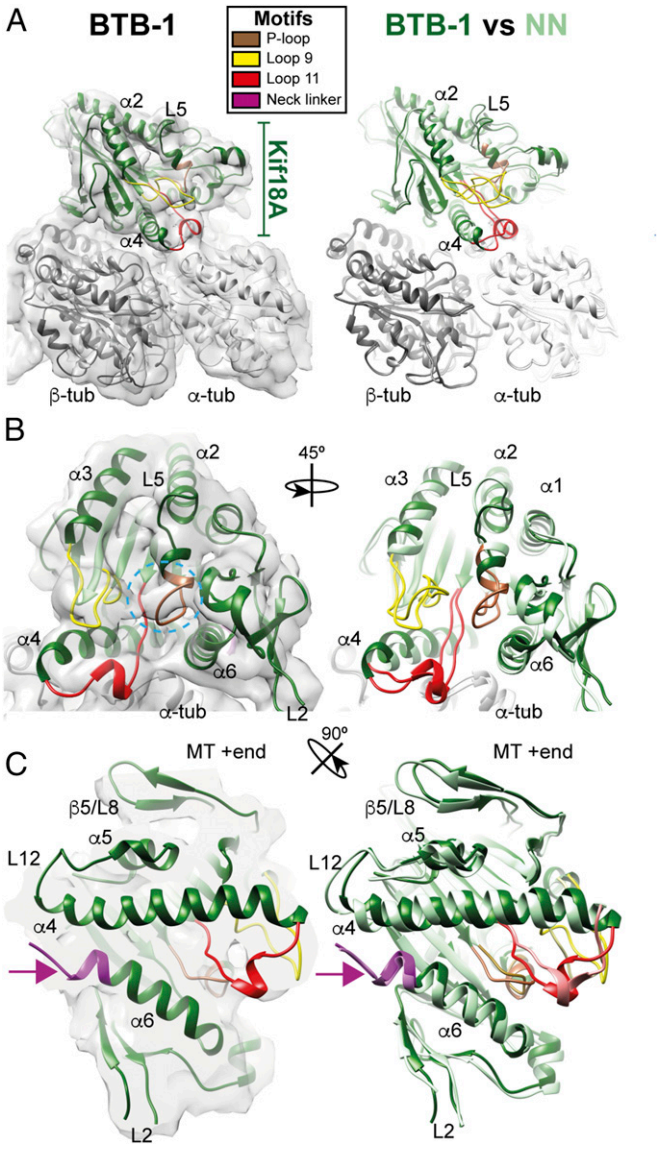

Fig. 5. Conformation of the MT-bound Kif18A motor domain in the presence of BTB-1. (*A*) Asymmetric unit from the Kif18A_MDNL BTB-1 reconstruction (*Left*) contoured to show secondary structural elements, and overlaid on the Kif18A_MDNL NN model (*Right*). The cryo-EM density is shown as a gray surface, the BTB-1 model is in dark-green ribbons, the NN model is in light-green ribbons, and α- and β-tubulin are in light- and dark-gray ribbons, respectively; (*B*) Changes in the nucleotide-binding pocket of Kif18A_MDNL in the presence of BTB-1 (*Left*) and BTB-1/NN overlay (*Right*). The arrow indicates that loop9 is in a similar conformation. (*C*) MT-binding interface of the BTB-1 reconstruction (*Left*) and BTB-1/NN overlay (*Right*), showing that this interface is similar in both structures. The arrow indicates that the C terminus of helix-α6 is essentially unchanged, with the neck linker undocked (in magenta).

To check whether this region is a favorable drug-binding pocket in Kif18A, we carried out a search for pockets accessible for small-molecule binding and favorable for interactions with methyl and aromatic probes (*SI Appendix*, Fig. S8*A*). Intriguingly, the top predicted pocket corresponds to the same region as identified in the difference map. To validate the pocket prediction and check the potential of this pocket for BTB-1 binding specifically, we modeled the Kif18A-BTB-1 complex using a two-step molecular docking protocol. A global search for BTB-1 binding with Haddock (45) identified poses for BTB-1 with the best energy score in the vicinity of this pocket (*SI Appendix*, Fig. S8*B*). The other proposed locations are either not in buried pockets or are far from the identified difference density. "Focused docking" performed at this potential binding site using both Haddock (45) (Fig. 6*C*) and AutoDock Vina (46) (Fig. 6*D*) and allowing side chain flexibility resulted in two similar binding modes. Following docking, cluster representatives from the 10 top-scoring poses based on Autodock Vina (unclustered) and the four top-scoring clusters based on Haddock (*SI Appendix*, Table S1), were selected. Finally, we proposed two docking poses based on the highest cross-correlation of BTB-1 (among the 14 poses) with both the difference and original densities (Fig. 6*E*). These two poses (one from Haddock and one from Autodock Vina) fit equally well, with Chimera CCC values of 0.86 and 0.86, respectively, with the difference map, and 0.73 and 0.75, respectively, with the original map (*SI Appendix*, Table S1).

BTB-1 specifically inhibits the activity of Kif18A compared with other kinesins (38). To investigate this, we first checked the conservation of interacting residues in the selected models of Kif18A-BTB-1 complex (*SI Appendix*, Fig. S9). Four residues (L124, M133, Y134, and T224, shown in red) in the binding site are rather specific to Kif18A (Fig. 6*E*), others (Y159, L207, N211, R214, and A230, shown in black) are shared with several other kinesin families, and the remainder (F232, L256, and D258, shown in blue) are highly conserved across the superfamily. While the resolution of our BTB-1–bound Kif18A_MDNL cryo-EM reconstruction is insufficient to directly visualize the residues involved in BTB-1 binding, computational analysis of the Kif18 model provides a strong indication of its binding site. The predicted binding site includes some Kif18A-specific residues, explaining the selectivity of BTB-1 inhibition.

To test this model of BTB-1 binding and inhibition of Kif18A, we mutated selected residues around the predicted BTB-1–binding pocket and tested the sensitivity of these mutants to BTB-1 inhibition in the MT gliding assay (Fig. 7). Unsurprisingly, given the dynamic nature of conformational changes in the motor in this region, the uninhibited activity of Kif18A_MDNL is sensitive to mutations in this region of the motor (Fig. 7*A*). Nevertheless, several point mutants of residues in this region (M133A, M133I, N211A, and R214A) exhibited reduced sensitivity to BTB-1 inhibition, as measured by gliding activity in the presence of BTB-1 compared with wild type (Fig. 7 *B* and *C*), whereas Y134P, which sits at the top of the predicted binding pocket, had almost no effect on the susceptibility to BTB-1 inhibition. These results support our proposed mechanism of Kif18A inhibition by BTB-1; on MT binding and ADP release, Kif18A undergoes conformational changes that create the binding pocket between helix-α2 and helix-α3. Once BTB-1 occupies this site, subdomain rearrangements that

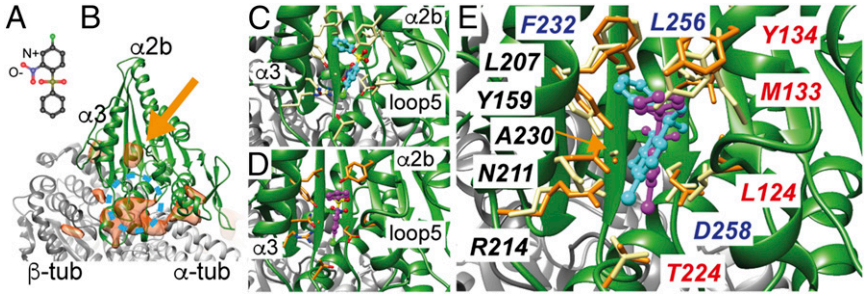

Fig. 6. Modeling of the putative BTB-1 binding site. (*A*) Depiction of BTB-1. (*B*) Difference in the cryo-EM density of NN vs. BTB-1 reconstructions (in orange) superimposed on the BTB-1–bound Kif18A_MDNL protein model. Much of the difference density corresponds to the previously described conformational differences around the nucleotide-binding site (dotted blue circle in Fig. 5 *A* and *B*), but an additional density peak (arrow) is located between helix-α2 and helix-α3, near loop5. (*C*) Zoom-in view of the BTB-1–binding pocket showing the Kif18A_MDNL protein model with the final docking pose (in turquoise) based on Haddock prediction. (*D*) Same view as in *B* but showing the Kif18A_MDNL protein model with the final docking pose (in purple) based on Autodock Vina predictions. (*E*) Same view as in *B* superposing final poses for BTB-1 from Haddock and Autodock Vina experiments. Kif18A-specific residues at this site, shared with few other kinesins, are labeled in red, moderately conserved residues among kinesin superfamily members are in black, and highly conserved residues are in blue (*SI Appendix*, Fig. S9).

would accompany ATP binding and support motor activity are blocked, trapping Kif18A on the MT.

Discussion

The complex machinery of the mitotic spindle is built from discrete populations of MTs. Each population is tightly regulated to perform specific functions and to collectively ensure the efficiency and accuracy of cell division. Kinesin-8s move processively along specific spindle MTs to reach their plus-ends and, on arrival, control MT plus-end dynamics; for example, kinetochore MTs are regulated by Kif18A to enable chromosome alignment before metaphase (11, 12). The dual activities of kinesin-8s—plus-end–directed stepping and ability to modulate MT dynamics—are encoded within the kinesin dimer, with the tail domain enhancing motor processivity, MT cross-linking activities, as well as MT end occupancy, thereby making significant contributions to motor function (13, 21, 24, 25, 47). However, our current structural and functional studies, together with previous cell biological work (43), also demonstrate that specific nucleotide-dependent conformational changes within the Kif18A monomeric motor domain are crucial for canonical plus-end stepping and for modulation of MT end dynamics.

We show that the major structural rearrangements within the Kif18A motor domain that drive plus-end–directed motility occur in the transition between the MT-bound NN and ATP-like states (Fig. 2). The closure of the nucleotide-binding site brings the surrounding conserved loops into a catalytically competent conformation, and induces extension of helix-α6 and reorientation of the neck linker toward the MT plus-end. Based on a previous, lower resolution Kif18A_MD reconstruction (29), we concluded that helix-α4 is bent in the Kif18A-MT complex. However, with the improved resolution of our current reconstructions, we can clearly see density corresponding to an extended helix-α4 in all nucleotide states; thus, the earlier conclusion arose owing to the limitations of the resolution. The conformational changes that we now see in our Kif18A_MDNL reconstructions are structurally conserved in multiple families of plus-end directed kinesins (31, 32, 39, 48). High-resolution structures of tubulin-bound kinesin-1 revealed that these changes arise from nucleotide-dependent subdomain rearrangements within the motor domain (31), and the models that we generated using available crystal structures are consistent with such conformational changes also occurring in Kif18A. Thus, in response to nucleotide binding, the main movements take place in the Switch I/II and P-loop subdomains with respect to the largely static tubulin-binding subdomain, which is centered on the continuous helix-α4 that binds the MT at the intradimer interface.

Our data show that the mechanism of MT depolymerization by the monomeric Kif18A motor domain is neither intrinsically limited to MT plus-ends nor dependent on processive stepping by dimers. Furthermore, our experiments reveal that Kif18A_MD is a weaker MT depolymerizer and forms rings much less readily than Kif18A_MDNL (Fig. 3 *A* and *B* and *SI Appendix*, Fig. S5 *A* and *B*). This difference in depolymerization activity implicates neck linker docking in conformational changes associated with modulation of MT end dynamics. However, surprisingly, the Kif18A_MD supports plus-end–directed motility in a gliding assay (Fig. 1*B*). We speculate that the ensemble nature of the gliding assay allows for the motile force generated by this truncated construct to be captured (49). The 2D profiles of the Kif18A_MDNL-MT-bound reconstruction and of Kif18A_MDNL within the tubulin rings are very similar (Fig. 3*E*), suggesting that ring formation involves similar subdomain rearrangements within the Kif18A motor domain in response to ATP— including neck linker docking—as seen on the MT lattice. This idea is also supported by the observation that both gliding and depolymerization are blocked by BTB-1 (Fig. 4). A very different structural mechanism for MT depolymerization was recently proposed for the kinesin-8 Kif19A (involved in length regulation of primary cilia) involving large-scale unfolding of the Kif19A motor domain (30); however, our data do not support such a mechanism in Kif18A.

Notably, comparison of the MT-bound Kif18A motor with the Kif18A crystal structure reveals a shift of loop8 and helix-α3 toward the MT surface (*SI Appendix*, Fig. S2). An equivalent conformational change has been reported previously (29) and in the motor domain of kinesin-8 Kif19A, which is also a dual-function motor (30), but not in kinesin-1, -3, or -5 (31, 32, 39, 50). Thus, this MT-induced conformational change may be specific for kinesin-8s, possibly as part of their adaptation to dual function on both the MT lattice and at MT ends. The work done by Kif18A_MDNL at the MT end (induction/stabilization of tubulin curvature) as opposed to the lattice (MT movement) is different because of the context; this is presumably achieved by responding to the relative deformability of the tubulin dimer to which the motor is attached. This suggests that the mechanochemistry of Kif18A is adaptable according to its molecular context.

In stabilizing curved tubulin oligomers, including rings, in the presence of AMPPNP, the depolymerization activity of Kif18A monomers appears similar to that of kinesin-13s (51–53). However, the depolymerization activity of Kif18A monomers is greater in the presence of AMPPNP than in the presence of ATP (Fig. 3*A*), clearly distinguishing it from the robust depolymerization capability of kinesin-13s in the presence of ATP (54). Thus, while the Kif18A monomeric motor has the ability to

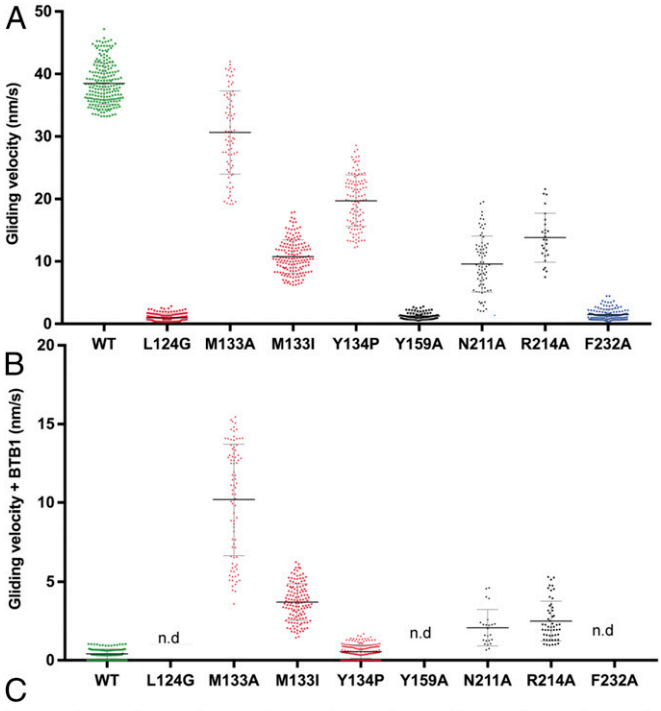

C

	WT	L124G	M133A	M133I	Y134P	Y159A	N211A	R214A	F232A
Gliding velocity (nm/s)	38.5 ± 3.3 (*n=208*)	1.0 ± 0.6 (*n=149*)	30.8 ± 6.6 (*n=78*)	10.8 ± 2.7 (*n=159*)	19.7 ± 4.1 (*n=112*)	1.3 ± 0.6 (*n=107*)	9.6 ± 4.5 (*n=72*)	13.8 ± 3.8 (*n=25*)	1.5 ± 0.9 (*n=123*)
Gliding velocity +BTB-1 (nm/s)	0.4 ± 0.6 (*n=139*)	n.d	10.2 ± 3.5 (*n=81*)	3.7 ± 1.2 (*n=131*)	0.6 ± 0.4 (*n=198*)	n.d	2.1 ± 1.2 (*n=23*)	2.5 ± 4.5 (*n=52*)	n.d
% vel. +BTB-1	**1.0**	-	**33**	**34**	**3.0**	-	**22**	**18**	-

Fig. 7. Effect of point mutations of Kif18A around the putative BTB-1–binding pocket on BTB-1 inhibition of MT gliding activity. (*A*) Effect of point mutation of residues around the proposed BTB-1– binding pocket on uninhibited Kif18A_MDNL MT gliding activity. The scatterplot shows all data, with mathematical mean ± SD indicated by horizontal bars. Data for WT are the same as in Fig. 1*C*. The difference between the activity of the mutant vs. WT Kif18A_MDNL was statistically significant for all proteins (*t* test, $P < 0.0001$). (*B*) Sensitivity of gliding activity of Kif18A_MDNL point mutants to inhibition by 50 μM BTB-1. The scatterplot shows all data, with mathematical mean ± SD indicated by horizontal bars. Data for WT are the same as in Fig. 4*C*. For mutants with defective motility (L124G, Y159A, and F232A), no additional data were collected in the presence of BTB-1. n.d, not done. (*C*) Summary of Kif18A_MDNL mutant gliding assay data showing the % gliding velocity in the presence of BTB-1 compared with the absence of BTB-1 for each mutant. The difference between inhibited and uninhibited activity was statistically significant for all proteins (*t* test, $P < 0.0001$).

induce/stabilize tubulin in a curved conformation, multiple motors may need to be retained at MT ends for depolymerization to occur. Below this threshold, however, accumulating Kif18A motors may influence MT dynamics by stabilizing a curved tubulin conformation, thereby inhibiting MT growth. Other motile kinesins also influence MT dynamics, for example, kinesin-4s that act as pausing factors at MT plus-ends (55, 56). The difference in depolymerization capacity in kinesin-8s compared with kinesin-13s may reflect a tunable mechanochemistry that exists across the kinesin superfamily encoded in their motor domains (43). In vivo, other factors work together with Kif18A on the ends of kinetochore MTs (e.g., ref. 57) to define the complex and tightly regulated dynamics of kinetochore MTs.

A recent investigation of the molecular mechanism of the Kip3 depolymerase (58) showed a number of parallels to our findings regarding Kif18A, highlighting the common mechanisms likely shared by kinesin-8s. The monomeric motor domains of these proteins, 50% identical by sequence, depolymerize MTs from both ends, demonstrating that depolymerization activity is likely intrinsic to kinesin-8 motor domains. As with Kif18A, the Kip3 neck linker makes an important contribution to its depolymerase activity. Furthermore, ATP binding rather than hydrolysis is sufficient for Kip3 depolymerase activity, as also demonstrated by our observation of faster depolymerization by Kif18A in the presence of AMPPNP compared with ATP. This work demonstrates the critical role of Kip3 loop11 for sensing MT ends, suppressing Kip3 ATPase activity, and promoting depolymerization. It also highlights the role of a specific residue in α-tubulin (equivalent in our complex to α-tubulin D116) in this depolymerization activity. In the Kif18A_MDNL-MT structure, the distance between loop11 residues and D116 is too far for a direct interaction (~14 Å), but curvature in the tubulin at MT ends—and as seen in our ring structures—likely would make interaction between these regions possible. While the structure of Kif18A in projection looks very similar in the rings and the lattice, a relatively small difference in the conformation of loop11 would not be detectable in our current 2D view of the rings. Thus, a similar role for Kif18A loop11 in modulating its depolymerization activity is not excluded by our data. It is possible that tubulin flexibility at MT ends supports the interaction between loop11 and this more distant region of α-tubulin; this in turn could lead to a subtle distortion of the catalytic site, suppressing motor ATPase activity while still allowing ATP binding. As a result, the subdomain rearrangements that are ordinarily coupled to ATPase hydrolysis on the MT lattice are instead used to facilitate tubulin's distortion or removal from MT ends. Further work on both Kif18A and Kip3 is needed to address this crucial mechanistic question.

We identified a potential binding site for the inhibitor BTB-1 between helix-α2 and helix-α3 of the Kif18A motor domain that is revealed due to MT-dependent subdomain movements. This region contains Kif18A-specific residues, explaining the specificity of BTB-1 for Kif18A inhibition compared with other mitotic kinesins (38). To accommodate BTB-1 in this region, the conformational shift of helix-α3 on MT binding is essential; the equivalent position in the MT-free Kif18A crystal structure is too small to accommodate BTB-1, providing a structural explanation for the specificity of BTB-1 for MT-bound Kif18A. BTB-1 thereby locks Kif18A in the MT-bound state (Fig. 8*A*), a mechanism that has been described as "gain-of-function" inhibition, in the sense that inhibited Kif18A gains a novel function of tight, rather than dynamic, MT binding (37) Although this kinesin inhibition mechanism is not strictly analogous to classical genetics gain-of-function mutations, it offers a useful point of comparison with Kif11 inhibitors (discussed below). The putative BTB-1– binding site lies at the junction of the SwI/II and P-loop subdomains that move with respect to each other when ATP binds (Fig. 2 and *SI Appendix*, Fig. S4). Thus, while BTB-1 inhibition is ATP-competitive, it acts allosterically by blocking the conformational changes that accompany ATP binding and reorganization of the catalytic site that enables ATPase activity. Our work provides a fresh perspective on the mechanism of Kif18A inhibition by BTB-1 that will be important for the development of novel small molecules capable of specifically inhibiting Kif18A in the cellular context (59).

Kif11 was the first kinesin for which a specific inhibitor — monastrol—was identified (35). Since then, numerous other allosteric inhibitors that bind to Kif11 loop5 have been developed and incorporated into cancer clinical trials (34). These compounds prevent tight MT binding (60), thereby blocking the force generation function of Kif11 within the spindle; that is, they work as "loss-of-function" inhibitors (37) (Fig. 8*B*). A similar mechanism

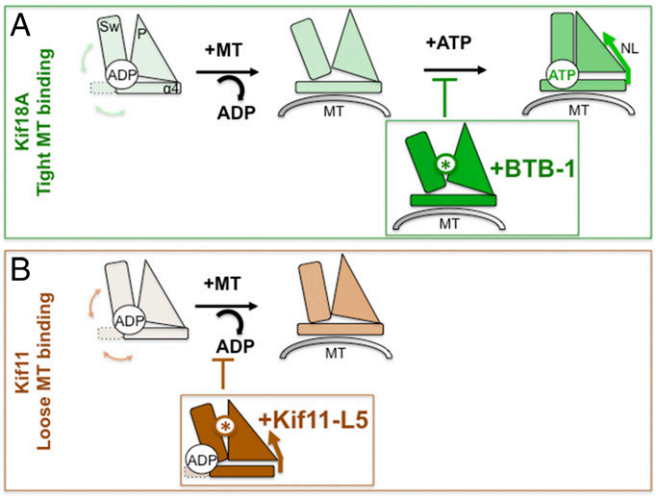

Fig. 8. Comparison of the structural basis of mitotic kinesin inhibition. (*A*) The mechanism of Kif18A inhibition by BTB-1 exemplifies a so-called gain-of-function kinesin inhibition mechanism. Here the SwI/II (Sw), P-loop (P), and tubulin-binding (represented by helix-α4, labeled α4) subdomains within the kinesin motor domain reorganize on MT binding (lattice or end) and ADP release to generate the Kif18A-NN state to which BTB-1 binds. BTB-1 binding locks Kif18A on the MT and also blocks ATP binding, ATP-dependent conformational changes, and consequent motor stepping. (*B*) The mechanism of Kif11 inhibition by loop5 (L5)-specific inhibitors, such as monastrol and ispinisib, exemplifies a loss-of-function kinesin inhibition mechanism. Here the inhibitors bind Kif11 off the MT and prevent the subdomain conformational changes required for tight MT binding and subsequent force generation.

also might operate in inhibitors for other mitotic kinesins—for example, the kinesin-14 HSET/KifC1, which is involved in MT clustering at spindle poles. A set of specific inhibitors have been designed to target HSET loop5 to block its activity in cancer cells and lead to apoptosis (61); however, redundancy within the spindle machinery can mean that such loss-of-function inhibition is prone to be overridden by other spindle components. Indeed, Kif15, a kinesin-12 with overlapping roles with Kif11 in mitotic MT organization, can functionally substitute for Kif11 in Kif11-independent dividing cells, thereby allowing the completion of mitosis in the absence of Kif11 (62, 63). The discovery of Kif11 inhibitors represented a paradigm shift in both the ability to functionally dissect the roles of kinesins in cell division and in establishing Kif11—and kinesins in general—as chemotherapeutic targets. Subsequent work has also highlighted the need to consider modes of kinesin inhibition that enhance MT binding to produce a mitotic block that is less readily overridden.

Such inhibition may be particularly advantageous for drugging the mitotic spindle. By trapping the target motor on its MT track and preventing its dynamic turnover, knock-on blockage of much of the dynamic spindle machinery can be achieved, thereby amplifying the antimitotic effect. In contrast to most Kif11 inhibitors and apart from the data presented here, to date no structural information is available about kinesin inhibitors that trap the motors on MTs, being by definition essentially largely inaccessible for study by X-ray crystallography. In addition to Kif18A inhibition by BTB-1, there are several reports of inhibitors of Kif11 that act allosterically and increase Kif11 MT binding within the spindle (37, 64). Similarly, the allosteric inhibitor (GSK923295) of CENP-E, a motor involved in metaphase chromosome alignment, blocks the release of inorganic phosphate from MT-bound CENP-E, and as demonstrated by mutagenesis and photolabeling, also binds in the vicinity of helix-α2, helix-α3, and loop5 (65). A series of selective HSET inhibitors that are ATP/ADP-competitive, specific for the motor's MT-bound state, and targeted to loop5 also have been described (66, 67). It seems likely that these inhibitors will work in a similar way and recognize specific sequences in this region of the particular motor. A recent study of inhibition of kinesin-1 by the general anesthetic propofol showed that kinesins active in interphase are also susceptible to perturbation of their ATPase cycles by small-molecule binding; this could be explained through mechanisms related to disruption of subdomain rearrangements (68). Thus, our study of BTB-1 inhibition of Kif18A reinforces a common mechanism of allosteric kinesin inhibition through binding at the dynamic interface of subdomains within the kinesin motor domain, either on or off the MT (69).

Mitotic kinesin inhibitors continue to be valuable tools for dissection of the mechanisms and roles of different motors within the complex spindle machinery, and may have clinical applications as well. The emergence of resistance to monotherapies by accumulation of point mutations presents a challenge to effective drug development and highlights the need to investigate multiple modes of mitotic motor inhibition to overcome drug resistance. The mechanistic redundancy intrinsic to mitosis highlights another problem with monotherapeutic approaches. Thus, the development of combinatorial drug therapies—in particular, inhibitors that trap motors tightly on MTs—in which several mitotic molecules are inhibited simultaneously is an important approach. This is critical to specifically inhibit collaborating or synergistic mitotic partners. In this context, work on Kif18A is relevant because it collaborates with CENP-E in chromosome alignment and is upregulated in a subset of cancers (19, 70). Thus, inhibitors like BTB-1 may be important when considered synergistically with CENP-E inhibition, particularly when considering the induction of CIN as a strategy for inducing tumor death (71). With the evolution of personalized treatments of heterogeneous cancers, the possibility of accurately targeting different components of the spindle in different ways is becoming increasingly important.

Materials and Methods

Protein Expression, Purification, and Labeling. Human Kif18A motor domain constructs were cloned into a pET28a vector (Novagen) containing a thrombin cleavable N-terminal His_6-tag and were expressed, purified, and biochemically characterized as described in *SI Appendix*.

Cryo-EM Sample Preparation, Data Collection, Processing, and Modeling. MTs were diluted in MT polymerization buffer (*SI Appendix, Materials and Methods*) to a final concentration of 10 or 20 μM polymerized tubulin, depending on the complex. In addition, 50 μM Kif18A_MDNL was incubated with 5 mM AMPPNP and kept at room temperature for 15 min, followed by incubation with 10 μM MTs before vitrification. For the NN complex, Kif18A_MDNL protein was incubated with Apyrase (10 units/mL; Sigma-Aldrich) for 10 min on ice and then warmed, followed by incubation with 10 μM MTs for another 15 min at room temperature. To form Kif18-tubulin rings for cryo-EM, Kif18A_MDNL was concentrated to 80 μM, mixed with 5 mM AMPPNP and 20 μM tubulin, and incubated for 30 min at room temperature before vitrification; this yielded samples with lower background compared with ring formation from depolymerizing MTs. Carbon grids (C-Flat 2/2 grids; Protochips) were glow-discharged in air, and 4 μL of each sample was applied. The grids were blotted with a final blotting step of 3.5 s and vitrified in liquid ethane using a Vitrobot Mark III (FEI) at 25 °C and 100% humidity. Images were collected manually on a 300-kV Tecnai G2 Polara microscope (FEI) equipped with a Quantum energy filter and K2 Summit direct electron detector (Gatan) in counting mode at a pixel size of 1.39 Å. Exposures were recorded at a total dose of ∼30 electrons $(Å^2)^{-1}$ s^{-1} over 10 s, with a defocus range of ∼0.5–3.5 μm. Details of the cryo-EM data processing and atomic modeling are provided in *SI Appendix*.

ACKNOWLEDGMENTS. We thank Anthony Roberts for help in designing the TIRF assays, access to the TIRF microscope, and very useful discussions. A.P.J. and M.T. also thank Joseph Newcombe, Martyn Winn, Ardan Patwardhan, and Ingvar Lagerstedt for useful technical discussions. J.L., A.P. and C.A.M. were supported by funding from Cancer Research UK (C33336/A13177) and Worldwide Cancer Research (16-0037), and thank Dr. Charles Sindelar (Yale University) for reconstruction algorithms. A.P.J. and M.T. are supported by the Medical Research Council, UK (MR/M019292/1 and MR/N009614/1). T.U.M. and M.M.M. were supported by funding from the Deutsch Forschungsgemeinschaft (CRC 969) and the Konstanz Research School of Chemical Biology.

1. Cross RA, McAinsh A (2014) Prime movers: The mechanochemistry of mitotic kinesins. *Nat Rev Mol Cell Biol* 15:257–271.
2. Welburn JP (2013) The molecular basis for kinesin functional specificity during mitosis. *Cytoskeleton* 70:476–493.
3. Wordeman L (2010) How kinesin motor proteins drive mitotic spindle function: Lessons from molecular assays. *Semin Cell Dev Biol* 21:260–268.
4. DeZwaan TM, Ellingson E, Pellman D, Roof DM (1997) Kinesin-related KIP3 of *Saccharomyces cerevisiae* is required for a distinct step in nuclear migration. *J Cell Biol* 138:1023–1040.
5. Gupta ML, Jr, Carvalho P, Roof DM, Pellman D (2006) Plus end-specific depolymerase activity of Kip3, a kinesin-8 protein, explains its role in positioning the yeast mitotic spindle. *Nat Cell Biol* 8:913–923.
6. Varga V, et al. (2006) Yeast kinesin-8 depolymerizes microtubules in a length-dependent manner. *Nat Cell Biol* 8:957–962.
7. Fukuda Y, Luchniak A, Murphy ER, Gupta ML, Jr (2014) Spatial control of microtubule length and lifetime by opposing stabilizing and destabilizing functions of kinesin-8. *Curr Biol* 24:1826–1835.
8. West RR, Malmstrom T, Troxell CL, McIntosh JR (2001) Two related kinesins, klp5^{+} and klp6^{+}, foster microtubule disassembly and are required for meiosis in fission yeast. *Mol Biol Cell* 12:3919–3932.
9. West RR, Malmstrom T, McIntosh JR (2002) Kinesins klp5(+) and klp6(+) are required for normal chromosome movement in mitosis. *J Cell Sci* 115:931–940.
10. Savoian MS, Gatt MK, Riparbelli MG, Callaini G, Glover DM (2004) *Drosophila* Klp67A is required for proper chromosome congression and segregation during meiosis I. *J Cell Sci* 117:3669–3677.
11. Mayr MI, et al. (2007) The human kinesin Kif18A is a motile microtubule depolymerase essential for chromosome congression. *Curr Biol* 17:488–498.
12. Stumpff J, von Dassow G, Wagenbach M, Asbury C, Wordeman L (2008) The kinesin-8 motor Kif18A suppresses kinetochore movements to control mitotic chromosome alignment. *Dev Cell* 14:252–262.
13. Weaver LN, et al. (2011) Kif18A uses a microtubule binding site in the tail for plus-end localization and spindle length regulation. *Curr Biol* 21:1500–1506.
14. Stout JR, et al. (2011) Kif18B interacts with EB1 and controls astral microtubule length during mitosis. *Mol Biol Cell* 22:3070–3080.
15. Tanenbaum ME, et al. (2011) A complex of Kif18b and MCAK promotes microtubule depolymerization and is negatively regulated by aurora kinases. *Curr Biol* 21:1356–1365.
16. Niwa S, et al. (2012) KIF19A is a microtubule-depolymerizing kinesin for ciliary length control. *Dev Cell* 23:1167–1175.
17. Kasahara M, et al. (2016) Clinicopathological relevance of kinesin family member 18A expression in invasive breast cancer. *Oncol Lett* 12:1909–1914.
18. Liao W, et al. (2014) High KIF18A expression correlates with unfavorable prognosis in primary hepatocellular carcinoma. *Oncotarget* 5:10271–10279.
19. Nagahara M, et al. (2011) Kinesin 18A expression: Clinical relevance to colorectal cancer progression. *Int J Cancer* 129:2543–2552.
20. Varga V, Leduc C, Bormuth V, Diez S, Howard J (2009) Kinesin-8 motors act cooperatively to mediate length-dependent microtubule depolymerization. *Cell* 138:1174–1183.
21. Su X, et al. (2011) Mechanisms underlying the dual-mode regulation of microtubule dynamics by Kip3/kinesin-8. *Mol Cell* 43:751–763.
22. Grissom PM, et al. (2009) Kinesin-8 from fission yeast: A heterodimeric, plus-end-directed motor that can couple microtubule depolymerization to cargo movement. *Mol Biol Cell* 20:963–972.
23. Erent M, Drummond DR, Cross RA (2012) *S. pombe* kinesins-8 promote both nucleation and catastrophe of microtubules. *PLoS One* 7:e30738.
24. Mayr MI, Storch M, Howard J, Mayer TU (2011) A non-motor microtubule binding site is essential for the high processivity and mitotic function of kinesin-8 Kif18A. *PLoS One* 6:e27471.
25. Stumpff J, et al. (2011) A tethering mechanism controls the processivity and kinetochore-microtubule plus-end enrichment of the kinesin-8 Kif18A. *Mol Cell* 43:764–775.
26. Möckel MM, Heim A, Tischer T, Mayer TU (2017) *Xenopus laevis* Kif18A is a highly processive kinesin required for meiotic spindle integrity. *Biol Open* 6:463–470.
27. Du Y, English CA, Ohi R (2010) The kinesin-8 Kif18A dampens microtubule plus-end dynamics. *Curr Biol* 20:374–380.
28. Kevenaar JT, et al. (2016) Kinesin-binding protein controls microtubule dynamics and cargo trafficking by regulating kinesin motor activity. *Curr Biol* 26:849–861.
29. Peters C, et al. (2010) Insight into the molecular mechanism of the multitasking kinesin-8 motor. *EMBO J* 29:3437–3447.
30. Wang D, et al. (2016) Motility and microtubule depolymerization mechanisms of the kinesin-8 motor, KIF19A. *Elife* 5:e18101.
31. Cao L, et al. (2014) The structure of apo-kinesin bound to tubulin links the nucleotide cycle to movement. *Nat Commun* 5:5364.
32. Shang Z, et al. (2014) High-resolution structures of kinesin on microtubules provide a basis for nucleotide-gated force generation. *Elife* 3:e04686.
33. Jordan MA, Wilson L (2004) Microtubules as a target for anticancer drugs. *Nat Rev Cancer* 4:253–265.
34. Rath O, Kozielski F (2012) Kinesins and cancer. *Nat Rev Cancer* 12:527–539.
35. Mayer TU, et al. (1999) Small molecule inhibitor of mitotic spindle bipolarity identified in a phenotype-based screen. *Science* 286:971–974.
36. Myers SM, Collins I (2016) Recent findings and future directions for interpolar mitotic kinesin inhibitors in cancer therapy. *Future Med Chem* 8:463–489.
37. Groen AC, et al. (2008) A novel small-molecule inhibitor reveals a possible role of kinesin-5 in anastral spindle-pole assembly. *J Cell Sci* 121:2293–2300.
38. Catarinella M, Grüner T, Strittmatter T, Marx A, Mayer TU (2009) BTB-1: A small molecule inhibitor of the mitotic motor protein Kif18A. *Angew Chem Int Ed Engl* 48:9072–9076.
39. Atherton J, et al. (2014) Conserved mechanisms of microtubule-stimulated ADP release, ATP binding, and force generation in transport kinesins. *Elife* 3:e03680.
40. Case RB, Rice S, Hart CL, Ly B, Vale RD (2000) Role of the kinesin neck linker and catalytic core in microtubule-based motility. *Curr Biol* 10:157–160.
41. Rice S, et al. (1999) A structural change in the kinesin motor protein that drives motility. *Nature* 402:778–784.
42. Topf M, et al. (2008) Protein structure fitting and refinement guided by cryo-EM density. *Structure* 16:295–307.
43. Kim H, Fonseca C, Stumpff J (2014) A unique kinesin-8 surface loop provides specificity for chromosome alignment. *Mol Biol Cell* 25:3319–3329.
44. Farabella I, et al. (2015) TEMPy: A Python library for assessment of three-dimensional electron microscopy density fits. *J Appl Cryst* 48:1314–1323.
45. van Zundert GCP, et al. (2016) The HADDOCK2.2 web server: User-friendly integrative modeling of biomolecular complexes. *J Mol Biol* 428:720–725.
46. Trott O, Olson AJ (2010) AutoDock Vina: Improving the speed and accuracy of docking with a new scoring function, efficient optimization, and multithreading. *J Comput Chem* 31:455–461.
47. Su X, et al. (2013) Microtubule-sliding activity of a kinesin-8 promotes spindle assembly and spindle-length control. *Nat Cell Biol* 15:948–957.
48. Goulet A, et al. (2012) The structural basis of force generation by the mitotic motor kinesin-5. *J Biol Chem* 287:44654–44666.
49. Vale RD, et al. (1996) Direct observation of single kinesin molecules moving along microtubules. *Nature* 380:451–453.
50. Goulet A, et al. (2014) Comprehensive structural model of the mechanochemical cycle of a mitotic motor highlights molecular adaptations in the kinesin family. *Proc Natl Acad Sci USA* 111:1837–1842.
51. Moores CA, et al. (2002) A mechanism for microtubule depolymerization by KinI kinesins. *Mol Cell* 9:903–909.
52. Tan D, Rice WJ, Sosa H (2008) Structure of the kinesin13-microtubule ring complex. *Structure* 16:1732–1739.
53. Asenjo AB, et al. (2013) Structural model for tubulin recognition and deformation by kinesin-13 microtubule depolymerases. *Cell Rep* 3:759–768.
54. Desai A, Verma S, Mitchison TJ, Walczak CE (1999) Kin I kinesins are microtubule-destabilizing enzymes. *Cell* 96:69–78.
55. Bringmann H, et al. (2004) A kinesin-like motor inhibits microtubule dynamic instability. *Science* 303:1519–1522.
56. Bieling P, Telley IA, Surrey T (2010) A minimal midzone protein module controls formation and length of antiparallel microtubule overlaps. *Cell* 142:420–432.
57. Ye F, et al. (2011) HURP regulates chromosome congression by modulating kinesin Kif18A function. *Curr Biol* 21:1584–1591.
58. Arellano-Santoyo H, et al. (2017) A tubulin binding switch underlies Kip3/kinesin-8 depolymerase activity. *Dev Cell* 42:37–51.e8.
59. Braun J, et al. (2015) Synthesis and biological evaluation of optimized inhibitors of the mitotic kinesin Kif18A. *ACS Chem Biol* 10:554–560.
60. Crevel IM, Alonso MC, Cross RA (2004) Monastrol stabilises an attached low-friction mode of Eg5. *Curr Biol* 14:R411–R412.
61. Watts CA, et al. (2013) Design, synthesis, and biological evaluation of an allosteric inhibitor of HSET that targets cancer cells with supernumerary centrosomes. *Chem Biol* 20:1399–1410.
62. Sturgill EG, Ohi R (2013) Kinesin-12 differentially affects spindle assembly depending on its microtubule substrate. *Curr Biol* 23:1280–1290.
63. Sturgill EG, Norris SR, Guo Y, Ohi R (2016) Kinesin-5 inhibitor resistance is driven by kinesin-12. *J Cell Biol* 213:213–227.
64. Chattopadhyay S, et al. (2015) Niche-based screening in multiple myeloma identifies a kinesin-5 inhibitor with improved selectivity over hematopoietic progenitors. *Cell Rep* 10:755–770.
65. Wood KW, et al. (2010) Antitumor activity of an allosteric inhibitor of centromere-associated protein-E. *Proc Natl Acad Sci USA* 107:5839–5844.
66. Wu J, et al. (2013) Discovery and mechanistic study of a small molecule inhibitor for motor protein KIFC1. *ACS Chem Biol* 8:2201–2208.
67. Yang B, et al. (2014) Discovery of potent KIFC1 inhibitors using a method of integrated high-throughput synthesis and screening. *J Med Chem* 57:9958–9970.
68. Bensel BM, et al. (2017) Common general anesthetic propofol impairs kinesin processivity. *Proc Natl Acad Sci USA* 114:E4281–E4287.
69. Scarabelli G, Grant BJ (2014) Kinesin-5 allosteric inhibitors uncouple the dynamics of nucleotide, microtubule, and neck-linker binding sites. *Biophys J* 107:2204–2213.
70. Huang HC, Shi J, Orth JD, Mitchison TJ (2009) Evidence that mitotic exit is a better cancer therapeutic target than spindle assembly. *Cancer Cell* 16:347–358.
71. Funk LC, Zasadil LM, Weaver BA (2016) Living in CIN: Mitotic infidelity and its consequences for tumor promotion and suppression. *Dev Cell* 39:638–652.